LIMNOLOGY and OCEANOGRAPHY

ASLO

Limnol. Oceanogr. 9999, 2024, 1–15

doi: 10.1002/lno.12656

Calcification increases carbon supply, photosynthesis, and growth in a globally distributed coccolithophore

Austin R. Grubb [1], **Christopher T. Johns** [1,a], **Matthew G. Hayden** [2], **Adam V. Subhas** [2], **Kimberlee Thamatrakoln** [1], **Kay D. Bidle** [1*]

[1]Department of Marine and Coastal Sciences, Rutgers University, New Brunswick, New Jersey, USA
[2]Department of Marine Chemistry and Geochemistry, Woods Hole Oceanographic Institution, Falmouth, Massachusetts, USA

Abstract

Coccolithophores fix organic carbon and produce calcite plates (coccoliths) that ballast organic matter and facilitate carbon export. Photosynthesis consumes carbon dioxide, while calcification produces it, raising questions about whether coccolithophores are a net sink or source of carbon. We characterized the physiology of calcified and noncalcified ("naked") phenotypes of *Emiliania huxleyi* (CCMP374) and investigated the relationship between calcification and photosynthesis across a gradient of light (25–2000 μmol photons m^{-2} s^{-1}) spanning the euphotic zone. Growth and photophysiological parameters increased with light until reaching a mid-light (150 μmol photons m^{-2} s^{-1}) maximum for both phenotypes. Calcified cells were characterized by enhanced photophysiology and less photoinhibition. Further, enhanced bicarbonate transport in calcified cells led to higher rates of particulate organic carbon fixation and growth compared to naked cells at mid-light to high light (150–2000 μmol photons m^{-2} s^{-1}). Coccolith production was similarly high at mid and high light, but the rate of coccolith shedding was >3-fold lower at high-light (1.2 vs. 0.35 coccoliths $cell^{-1}$ h^{-1}). The cellular mechanims(s) of this differential shedding remain unknown and underly light-related controls on coccosphere maintenance. Our data suggest coccoliths shade cells at high light and that enhanced bicarbonate transport associated with calcification increases internal carbon supplies available for organic carbon fixation.

Coccolithophores are eukaryotic phytoplankton that contribute to the global carbon cycle through the production of particulate organic carbon (POC) and calcification, a light-dependent process that produces particulate inorganic carbon (PIC) in the form of calcium carbonate ($CaCO_3$) plates known as coccoliths (Paasche 2002). Globally, coccolithophores account for at least half of the annual 80–120 Tmol of PIC produced in the pelagic ocean (Westbroek et al. 1993; Balch et al. 2007; Berelson et al. 2007; Broecker and Clark 2009; Ziveri et al. 2023) with coccoliths representing ~50% of the calcite reaching the seafloor (Broecker and Clark 2009). Given $CaCO_3$ is denser and experiences less water column dissolution than biogenic silica, it is responsible for up to 83% of the carbon flux to depth globally (Klaas and Archer 2002). Fluctuations in PIC production by coccolithophores under different environmental conditions will alter the ballasting present in surface ocean communities, with important implications for biological pump efficiency (Armstrong et al. 2001; Klaas and Archer 2002; Ridgwell et al. 2009).

Energetic costs of calcification are estimated at one-third of the total cellular photosynthetic energy budget, with the cost likely scaling with the degree of calcification across species and environmental conditions (Monteiro et al. 2016). Calcification takes place in a coccolith deposition vesicle (Young and Henriksen 2003) and consumes bicarbonate (HCO_3^-) while producing carbon dioxide (CO_2). This has led to the hypothesis that calcification acts as a localized, intracellular carbon concentrating mechanism (CCM), accelerating photosynthetic carbon fixation (i.e., light-independent or "dark" reactions, DR) (Paasche 1964; Nimer et al. 1997; Buitenhuis et al. 1999; Bach et al. 2013; Kottmeier et al. 2014). Coccoliths may also benefit photosynthesis by optically funneling photons into

*Correspondence: bidle@marine.rutgers.edu

[a]Present address: B CUBE, Center for Molecular Bioengineering, Technische Universität Dresden, Dresden, Germany

Additional Supporting Information may be found in the online version of this article.

Author Contribution Statement: ARG, KT, and KDB planned and designed the research. ARG, CTJ, MGH, AVS, and KDB performed experiments. ARG, AVS, KT, and KDB analyzed the data. ARG, KT, and KDB wrote the manuscript and CTJ and AVS provided comments.

the cell and making more light available for the light-dependent reactions (LR) of photosynthesis (Monteiro et al. 2016). Alternatively, coccoliths may protect the cell from photodamage by optically scattering photosynthetic active radiation (PAR) and UV light at the cell surface and/or dissipating light energy inside the cell (Guan and Gao 2010; Barcelos e Ramos et al. 2012; Monteiro et al. 2016).

Light is a major determinant of coccolithophore biogeography and is essential for bloom formation (Nanninga and Tyrrell 1996). Blooms of *Emiliania huxleyi*, the most abundant and widely distributed coccolithophore, occur primarily in stratified, high-latitude regions in the upper 10–20 m of the ocean and at irradiances of 280–600 μmol photons m^{-2} s^{-1} (Iglesias-Rodríguez et al. 2002; Rost and Riebesell 2004; Tyrrell and Merico 2004). Although calcification has been shown to be light-dependent (Paasche 2002), the impact of irradiance on calcification is unclear. Calcification becomes limited in *E. huxleyi* below 30 μmol photons m^{-2} s^{-1} (Raven and Crawfurd 2012), leading to low PIC and POC fixation rates and low cellular PIC : POC quotas (van Bleijswijk et al. 1994; Balch et al. 1996; Paasche 1999). Balch et al. (1996) concluded that the DR of photosynthesis and calcification are decoupled at low irradiance where growth is light limited. Calcification increases with light, saturating at lower irradiances than photosynthesis ($\sim$ 72 to > 500 μmol photons m^{-2} s^{-1}; Paasche 1964; Balch et al. 1992; Trimborn et al. 2007). This leads to POC fixation outpacing PIC production and decreasing the PIC : POC ratio at high light conditions (Raven and Crawfurd 2012; Krumhardt et al. 2017). Although it is unclear if calcification or photosynthesis is photoinhibited at higher irradiances (Paasche 1964; Balch et al. 1992; Trimborn et al. 2007; Feng et al. 2008), growth of *E. huxleyi* appears resistant to photoinhibition (up to $\sim$ 800 μmol photons m^{-2} s^{-1}), regardless of calcification state (Paasche 2002).

Emiliania huxleyi is a model system for studying the collective impact of photosynthesis and calcification on the carbon cycle, in part due to its global distribution and the availability of both calcified and naked strains. The pan genome of *E. huxleyi* and extensive intraspecific diversity, including genetic and physiological differences unrelated to calcification (Read et al. 2013), complicates the interpretation of physiological differences between strains. Some studies have attempted to resolve this issue by manipulating the calcification state by altering the calcium concentration in growth media (Johns et al. 2019; Herfort et al. 2004; Trimborn et al. 2007; Nam et al. 2018) or chemically treating cells with Ca^{2+} chelators and/or acid to remove the coccoliths (de Jong et al. 1976; Balch et al. 1996; Lyon 2014). However, these chemical manipulations can impact cell physiology unrelated to calcification leading an incomplete understanding of the role of calcification and its ecophysiological trade-offs (Monteiro et al. 2016).

Here, we acclimated previously described naked and calcified phenotypes that were derived from the same genotype of *E. huxleyi* CCMP374 (Johns et al. 2019, 2023) to a range of irradiances (25–2000 μmol photons m^{-2} s^{-1}) to elucidate the interplay between light, photosynthesis, and calcification. Calcification was assessed using flow cytometry, particulate carbon measurements, ^{14}C radioisotope incubations, ^{13}C stable isotope analyses, and analyses of media carbonate chemistry. Respective LR and DR of photosynthesis were interrogated via biophysical measurements and ^{14}C incubations coupled with microdiffusion (Paasche and Brubak 1994; Balch et al. 2000). Furthermore, immunoblot analysis of key photosynthetic proteins was used to quantify the relative investment in photosynthetic machinery between phenotypes and across irradiances. Taken together, our data provide a cellular context for calcification and the role of coccolithophores in the carbon cycle.

Materials and methods

Strains and culture conditions

A clonal, noncalcified ("naked") phenotype of *E. huxleyi* CCMP374 (originally isolated from the Gulf of Maine in 1990; National Center for Marine Algae and Microbiota; https://ncma.bigelow.org/CCMP374) was rendered calcified by culturing under P-limiting conditions (N : P of 240 : 1) for > 8 months. It remained stably calcified for > 3 yr after transfer back into replete *f*/2 minus Si medium (*f*/2 − Si) (Johns et al. 2019, 2023). Genetic similarity of the naked and calcified phenotypes was assessed via microsatellite analysis (Supporting Information Fig. S1; Table S1). Monoclonal, nonaxenic cultures were maintained at 18°C on a 14 : 10 light : dark cycle at different irradiances (25, 150, 500, 1000, and 2000 μmol photons m^{-2} s^{-1}) using white fluorescence lighting (T5, Sylvania DULUX L 55W and T8, Philips Alto II 17W) and maintained optically thin (< 5×10^5 cells mL^{-1}) in steady-state exponential growth by frequent transfers into fresh media (c. 2–4 d) for > 12 months prior to experimentation.

Cell enumeration

Cell concentration was measured by flow cytometry (BD Accuri C6, BD Biosciences). Growth rates (μ, d^{-1}) were calculated as $\mu = (\ln(N_2) - \ln(N_1))/(t_2 - t_1)$, where N_1 is the cell concentration (cells mL^{-1}) at time t_1, N_2 is the cell concentration at time t_2. Doubling times (t_d, d) were determined from growth rates by $t_d = (1/\mu) \times \ln(2)$.

Particulate carbon measurements

Cellular POC and PIC quotas were assessed using a CNS Elemental Analyzer (Carlo Erba NA 1500). Cells were collected $\sim$ 4–6 h into light phase via filtration onto precombusted GF/F filters (× 6) and stored at −20°C. After drying at 60°C, three filters for POC measurements were exposed to 10% HCl fumes in a glass desiccator overnight to dissolve and volatize the PIC. The remaining three filters were untreated and represented total particulate carbon (TPC). Particulate inorganic carbon quotas were determined by the difference between TPC and POC divided by the number of cells. Coccolith PIC

content was measured using a CNS Elemental Analyzer after isolating coccoliths (Gal et al., 2016; Johns et al. 2023).

Assessing calcification via flow cytometry

Calcification was assessed optically via flow cytometry; calcified cells (organic cell plus coccosphere) have an order of magnitude higher side scatter (SSC) than naked cells (organic cell alone) (von Dassow et al. 2012; Johns et al. 2019). Free coccoliths were counted using an Influx Model 209S Mariner flow cytometer (BD Biosciences) using Brewster angle optics as previously described (Johns et al. 2019, 2023). Coccolith shedding rates were determined by sampling live calcified cell cultures and immediately measuring the cell-normalized free coccolith populations over a 4.5-h period in the middle of the light phase. Coccolith shedding rates were calculated by fitting a linear regression to the data for each biological replicate.

Measurements of the LR of photosynthesis

Chlorophyll *a* (Chl *a*) was extracted from filters in 90% acetone and Chl *a* concentrations were determined via absorbance according to (Jeffrey and Humphrey 1975; *see* Supporting Information for details). Fluorescence-based photosynthetic measurements were performed using a custom-built fluorescence induction and relaxation system (FIRe; Gorbunov and Falkowski 2005). Fluorescence measurements were used to determine: the maximum photochemical quantum yield of photosystem II (PSII) (Kitajima and Butler 1975); the maximum rate of photosynthetic electron transport (ETR_{max}); light saturation irradiance (E_k) from reconstructions of photosynthesis vs. irradiance curves (PE; Jassby and Platt 1976; Silsbe and Kromkamp 2012); and thermal dissipation of photons via nonphotochemical quenching (NPQ; Bilger and Björkman 1990). See Supporting Information for details.

Quantitative immunoblot analysis

Protein extraction and quantitative immunoblots were performed as previously described (Brown et al. 2008; Thamatrakoln et al. 2013). See Supporting Information for details.

Particulate carbon production rates

Particulate organic carbon (i.e., DR of photosynthesis) and PIC production rates were measured using ^{14}C-labeled sodium bicarbonate and the microdiffusion technique (Paasche and Brubak 1994; Balch et al. 2000). Briefly, 10 mL cultures were spiked with 5 μCi (185,000 Bq) of ^{14}C-labeled sodium bicarbonate and incubated at 25, 150, or 2000 μmol photons $m^{-2}\ s^{-1}$ for either 3 h or 24 h. The 3-h incubations were conducted in the middle of the light phase when the PE curve-derived ETR_{max} was constant. The 24-h incubations began at the start of the light phase and concluded at the end of the dark phase. Incubations were terminated and samples were processed via microdiffusion according to Paasche and Brubak (1994) and Balch et al. (2000) (*see* Supporting Information for details). Particulate inorganic carbon and POC fixation rates were calculated according to Parsons et al. (1984) and Paasche and Brubak (1994) (*see* Supporting Information for details). Particulate inorganic carbon production rates were also calculated from alkalinity drawdown and $\delta^{13}C$ values of PIC were determined using established methods (*see* Supporting Information for details on *Carbonate system characterization*). Particulate inorganic carbon production rates, coccolith PIC content, and coccolith shedding rates were used to determine coccosphere PIC quotas and fraction of coccoliths and PIC discarded via shedding (*see* Supporting Information for details on *Coccosphere and coccolith calculations*).

Statistical analysis

Statistical analyses were performed using the R stats package (version 3.6.3; *see* Supporting Information Dataset S1 for detailed analyses). Significance at a given irradiance between phenotypes was determined by independent, two-tailed *t*-test of equal variance (*t.test* function). Significance of trends over irradiance within a phenotype was determined by ANOVA (*aov* function) followed by a Tukey (honestly significant difference [HSD]) post hoc test (*TukeyHSD* function) to identify where significant differences occurred.

Results

Calcification increases with growth irradiance

Scanning electron microscopy analysis confirmed calcification in cells grown across light levels between 25 and 2000 μmol photons $m^{-2}\ s^{-1}$ (Supporting Information Fig. S2a). Calcified cells had higher mean side scatter (SSC), ranging from 8.8×10^5 to 2.0×10^6 arbitrary units (AU) compared to naked cells, which ranged from 7.8×10^4 to 1.3×10^5 AU (*t*-tests *p*-value < 0.001; Supporting Information Dataset S1). Greater than 95% of the population showed calcified SSC signatures in calcified cultures (Fig. 1a; Supporting Information Fig. S3). Cellular PIC quotas, measured via two distinct methods (*see* Materials and Methods), confirmed SSC signatures in calcified cells; quotas at 25 μmol photons $m^{-2}\ s^{-1}$ were 3.4 ± 0.6 pg C $cell^{-1}$ and increased to 8.4 ± 0.93–9.0 ± 2.9 pg C $cell^{-1}$ at 150, 500, and 2000 μmol photons $m^{-2}\ s^{-1}$ (ANOVA *p*-value < 0.001; Tukey HSD *p*-value < 0.05; Fig. 1b; Supporting Information Dataset S1).

The ratio of free coccolith : cell (Fig. 1c), a proxy for coccolith production, was lowest for cells grown at 25 μmol photons $m^{-2}\ s^{-1}$, with a median free coccolith : cell ratio of 4.3 (ANOVA *p*-value < 0.001; Tukey HSD *p*-value < 0.05; Fig. 1c; Supporting Information Dataset S1). This increased 3-fold at 150 μmol photons $m^{-2}\ s^{-1}$ and remained high up to 2000 μmol photons $m^{-2}\ s^{-1}$ (Fig. 1c; Supporting Information Dataset S1). This pattern was also reflected in cell size and coccolith dimensions. At 25 μmol photons $m^{-2}\ s^{-1}$, calcified cells were 4.3 ± 0.03 μm and increased to ~ 5.4 μm at 150 and 2000 μmol photons $m^{-2}\ s^{-1}$

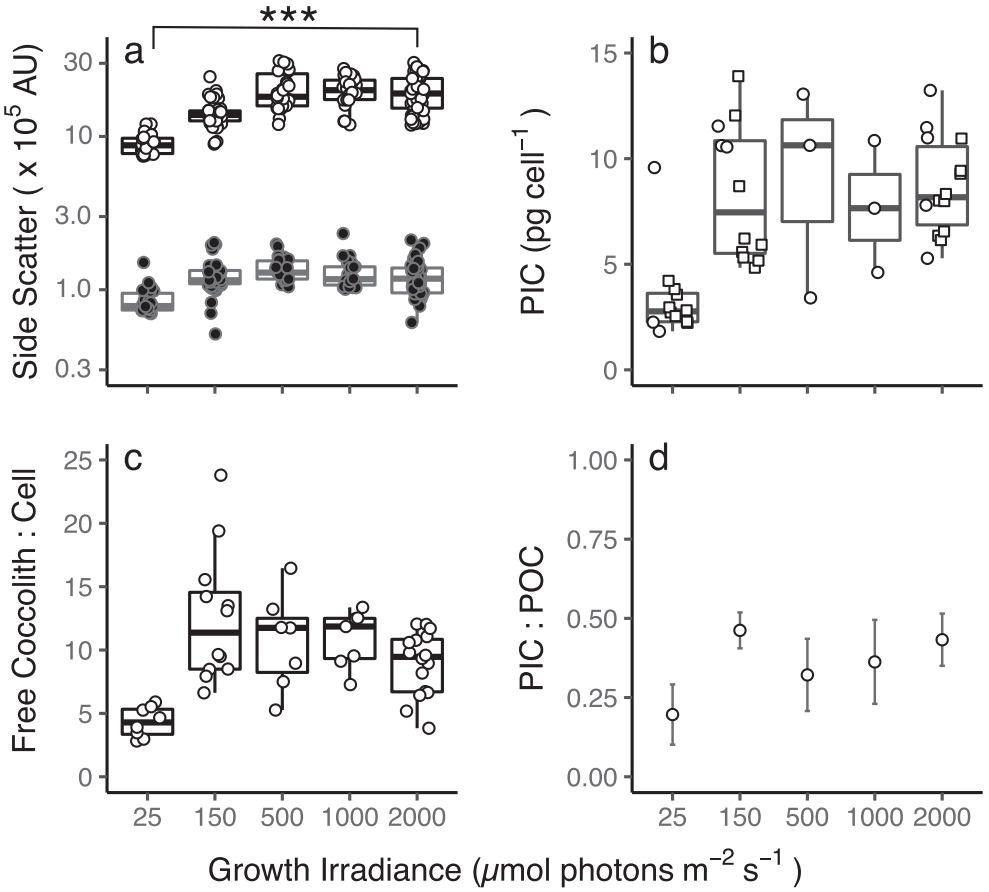

Fig. 1. Calcification state across a range of acclimated growth irradiances. Side scatter (SSC) signatures (**a**) of naked (closed, $n = 22$–51) and calcified (open, $n = 24$–51) cell cultures (***$p < 0.001$ at each irradiance), cellular particulate inorganic carbon (PIC) quota (**b**), and free coccolith : cell ratio (**c**; $n = 7$–20) for cells grown at 25–2000 μmol photons m^{-2} s^{-1}. Cellular PIC quotas (b) were determined using the by difference method (circles, $n = 3$) and directly measuring carbon liberated from PIC (squares, $n = 9$; *see* Materials and Methods). Cellular particulate organic carbon (POC) (Supporting Information Fig. S4) and PIC quotas (from by difference method) were used to determine the PIC : POC ratio (**d**) for calcified cells. Upper and lower bounds of each box plot in (**a**), (**b**), and (**c**) represent the 25th and 75th percentiles around the median, with whiskers representing data that are ≤ 1.5 times the interquartile range. Data beyond this range are outliers. The mean and standard error for panels (**d**) are shown ($n = 3$). There was no PIC detected for naked cells so closed circles are not included in (**b**–**d**). See Supporting Information Dataset S1 for statistical comparisons across irradiances.

(ANOVA p-value < 0.001; Tukey HSD p-value < 0.001). Cell size of naked cells followed a similar trend but was ~ 7–14% smaller than calcified cells (ANOVA p-value < 0.001; Tukey HSD p-value < 0.001; Supporting Information Fig. S2e). Coccolith length and width were also lowest at 25 μmol photons m^{-2} s^{-1} and increased by ~ 17% and ~ 31%, in cells grown at 150 and 2000 μmol photons m^{-2} s^{-1}, respectively (ANOVA p-value < 0.001; Tukey HSD p-value < 0.001; Supporting Information Fig. S2b,c). Coccolith PIC content was similar at 25 and 2000 μmol photons m^{-2} s^{-1} (0.30 ± 0.02 and 0.27 ± 0.02 pg C coccolith^{-1}, respectively), but decreased at 150 μmol photons m^{-2} s^{-1} (0.20 ± 0.02 pg C coccolith^{-1}; ANOVA p-value < 0.05; Tukey HSD p-value < 0.05; Supporting Information Fig. S2d).

Cellular POC quotas were similar between naked (19.6 ± 1.7 to 26.8 ± 5.1 pg C cell^{-1}) and calcified cells (22.3 ± 2.6 to 29.4 ± 1.9 pg C cell^{-1}) and did not significantly change across irradiance (Supporting Information Fig. S4; Dataset S1). In calcified cells, the ratio of PIC : POC did not significantly change across irradiance (0.20 ± 0.10 to 0.46 ± 0.06; Fig. 1d).

Comparative growth rates across irradiances

The steady-state, specific growth rate (μ; d^{-1}) followed similar trends for naked and calcified cells as irradiance increased (Fig. 2). The lowest μ was observed at 25 μmol photons m^{-2} s^{-1}, with a median of 0.31 and 0.27 d^{-1} for naked and calcified cells, respectively (ANOVA p-value < 0.001; Tukey HSD p-value < 0.001). The highest median μ was observed at 150 and 500 μmol photons m^{-2} s^{-1} for naked (0.87 and 0.93 d^{-1}, respectively) and calcified (1.00 and 0.98 d^{-1}, respectively) cells. Growth rates decreased at 1000 and 2000 μmol photons m^{-2} s^{-1} to 0.69 and ~ 0.81 d^{-1} for naked and

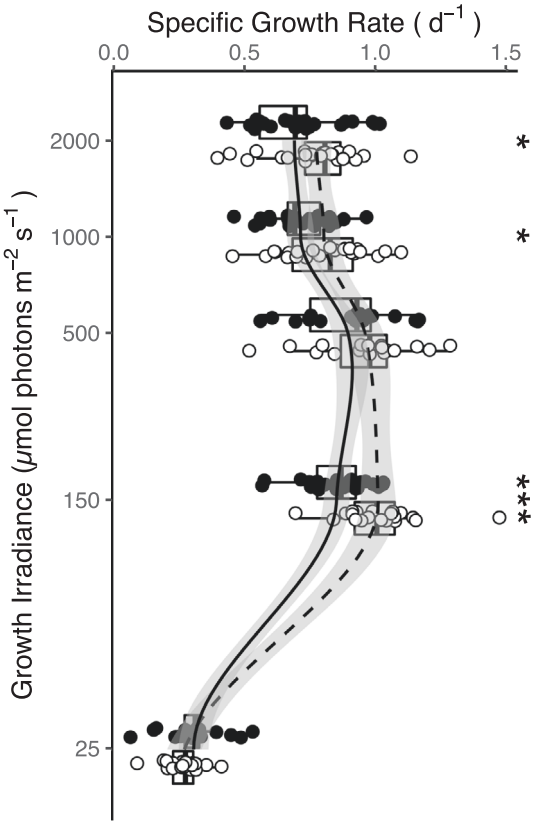

Fig. 2. Steady-state growth rates of naked and calcified cells across a range of growth irradiances. Data show general relationships across photic zone light intensities with irradiance plotted on a $\log_{10}$ scale. Depths are not presented, given the vertical attenuation coefficient of light (Kd) will change with location and water column properties, but the pattern would still be applicable across different regimes. Closed and open symbols represent naked ($n = 19$–32) and calcified ($n = 18$–27) cultures, respectively. Upper and lower bounds of each box plot represent the 25th and 75th percentiles around the median, with whiskers representing data that are ≤ 1.5 times the interquartile range. Data beyond this range are outliers. Solid (naked) and dashed (calcified) curve fits represent LOESS lines of best fit (span = 0.4; shaded area = 95% confidence interval) and shows the general trends of μ across growth irradiance. Asterisks indicate pairwise statistical differences (*$p < 0.05$ and ***$p < 0.001$, respectively) between naked and calcified cell cultures. See Supporting Information Dataset S1 for statistical comparisons across irradiances.

calcified cells, respectively (Tukey HSD p-value < 0.05). The median μ was significantly lower for naked cells than calcified cells at 150, 1000, and 2000 μmol photons m^{-2} s^{-1} (naked: 0.87, 0.69, and 0.69 d^{-1}, respectively; calcified 1.0, 0.83, and 0.81 d^{-1}, respectively; t-tests p-value < 0.05; Fig. 2; Supporting Information Dataset S1). The general relationship between μ and growth irradiance was visualized using a LOESS analysis of best fit. Naked and calcified cells clustered into low (LL, 25 μmol photons m^{-2} s^{-1}), medium (ML, 150–500 μmol photons m^{-2} s^{-1}), and high (HL, 1000–2000 μmol photons m^{-2} s^{-1}) light designations for more detailed downstream analyses.

The impact of irradiance on photophysiology

Chlorophyll *a* and biophysical measurements were used to assess the impact of light and calcification on photophysiology (Fig. 3; Supporting Information Fig. S5). Chlorophyll *a* quotas decreased with irradiance in naked and calcified cells (ANOVA p-value < 0.001), from 0.19 ± 0.004 and 0.19 ± 0.008 pg Chl *a* cell^{-1} at LL to 0.05 ± 0.003 and 0.07 ± 0.008 pg Chl *a* cell^{-1} at HL, respectively (Fig. 3a; Supporting Information Dataset S1). The maximum photochemical quantum yield of PSII (F_v/F_m) was highest at LL for both phenotypes (0.42 and 0.43 for naked and calcified cells, respectively) and decreased with irradiance (ANOVA p-value < 0.001) to lowest values at HL, where naked cells had a lower F_v/F_m than calcified cells (0.20 and 0.32, respectively; t-test p-value < 0.001; Fig. 3b).

The maximum photosynthetic electron transport rates per PSII (ETR_{max}) increased in naked cells from LL to ML (ANOVA p-value < 0.001, Tukey HSD p-value < 0.01) and saturated at HL; minimum and maximum median ETR_{max} were 201 and 1427 e$^-$ s^{-1} PSII^{-1}, respectively (Fig. 3c; Supporting Information Fig. S5c). ETR_{max} followed a similar pattern in calcified cells, significantly increasing from LL to HL (287–1623 e$^-$ s^{-1} PSII^{-1}; ANOVA p-value < 0.001, Tukey HSD p-value < 0.001; Fig. 3c; Supporting Information Fig. S5c) but was not statistically different than ETR_{max} in naked cells at any light level.

The saturation irradiance of photosynthesis (E_k) increased with growth irradiance in both cell types (ANOVA p-value < 0.001; Supporting Information Fig. S5d), while the ratio of E_k to growth irradiance (E_k/E) decreased (ANOVA p-value < 0.001; Fig. 3d; Supporting Information Fig. S5d). E_k was significantly higher in calcified cells than naked cells at LL (62 vs. 39 μmol photons m^{-2} s^{-1}, t-test p-value < 0.05), but lower at HL (487 vs. 646 μmol photons m^{-2} s^{-1}, t-test p-value < 0.05; Supporting Information Fig. S4; Dataset S1). This resulted in significant differences in E_k/E for naked and calcified cells at LL (1.6 and 2.5, respectively) suggesting calcified cells experienced more light limitation than naked cells. Photosynthesis rates for both phenotypes appeared to be optimal at ML as $E_k/E \sim 1$ (Fig. 3d). Both phenotypes grown at HL had lower E_k/E, indicating photosynthesis was light-saturated (Tukey HSD p-value < 0.05; Fig. 3d; Supporting Information Fig. S5d).

The initial slope of the PE curve (α) was similar at LL and ML in both cell phenotypes but decreased at HL (Supporting Information Fig. S5f). α was indistinguishable between phenotypes at LL and ML, but was significantly lower in naked cells compared to calcified cells at HL (t-test p-value < 0.05; Supporting Information Dataset S1).

The functional absorptive cross section (σ_{PSII}) in naked cells showed a ML maximum of 1061 Å^2, which was significantly higher than LL (985 Å^2; ANOVA p-value < 0.001; Tukey HSD p-value < 0.05) and HL (507 Å^2; Tukey HSD p-value < 0.001; Fig. 3e). Likewise, σ_{PSII} in calcified cells was maximal at ML (1052 Å^2); it was 15% smaller at LL (892 Å^2; ANOVA p-value

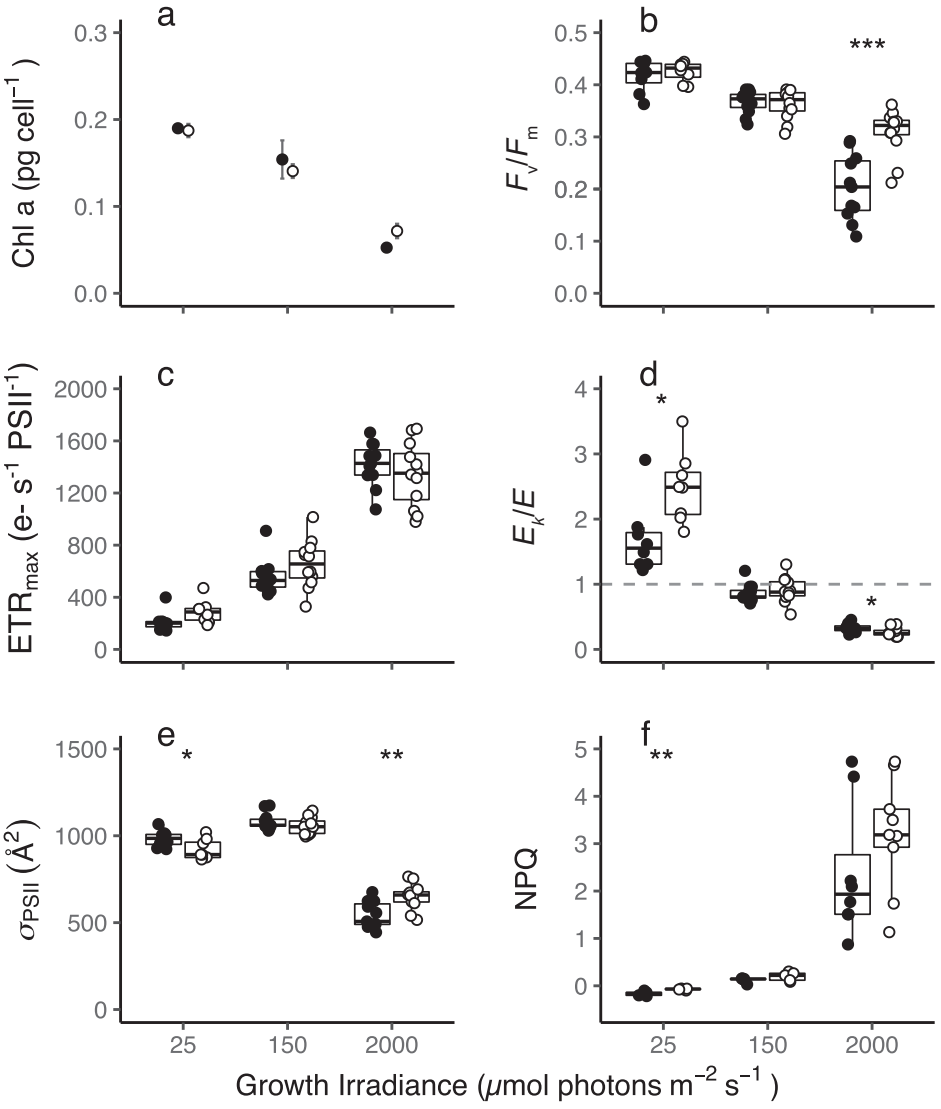

Fig. 3. Photosynthetic parameters for acclimated cells across irradiance levels. Cellular chlorophyll *a* (Chl *a*) quotas (**a**), photosynthetic efficiency, F_v/F_m (**b**), photosystem II (PSII)-normalized maximum electron transport rates, ETR_{max} (**c**), saturation irradiance to growth irradiance, E_k/E (**d**), functional absorptive cross section of PSII, σ_{PSII} (**e**), and nonphotochemical quenching, NPQ, (**f**) for naked (closed circles) and calcified (open circles) cells. In (**a**), the mean and standard error are shown ($n = 2$–6). Upper and lower bounds of each boxplot represent the 25th and 75th percentiles around the median ($n = 8$–12), with whiskers representing data that are ≤ 1.5 times the interquartile range. Data beyond this range are outliers. Asterisks indicate pairwise statistical differences (*$p < 0.05$; **$p < 0.01$; ***$p < 0.001$) between naked and calcified cell cultures within each irradiance. Statistical comparisons across irradiances are available in Supporting Information Dataset S1.

< 0.001; Tukey HSD *p*-value < 0.001) and 37% lower at HL (659 Å^2; Tukey HSD *p*-value < 0.001). Within irradiance levels, calcified cells maintained significantly lower (10% at LL; *t*-test *p*-value < 0.05) and higher (30% at HL, *t*-test *p*-value < 0.01; Fig. 3e) σ_{PSII} compared to naked cells.

Nonphotochemical quenching was undetectable at LL for both cell types but significantly increased from < 1 at ML to 1.9 and 3.2 at HL in naked and calcified cells, respectively (ANOVA *p*-value < 0.001; Tukey HSD *p*-value < 0.05; Fig. 3f). There were no significant differences between naked and calcified cells at any irradiance (Fig. 3f; Supporting Information Dataset S1).

Investments in photosynthetic machinery

Quantitative immunoblots of PsbD and RbcL determined respective photosynthetic investments in electron transport (PSII) and carbon fixation (RuBisCO). In naked cells, cellular PsbD quota was similar across irradiance, ranging from 0.54 ± 0.03 amol cell^{-1} at LL to 0.43 ± 0.06 amol cell^{-1} at HL. In contrast, PsbD quotas in calcified cells decreased at HL

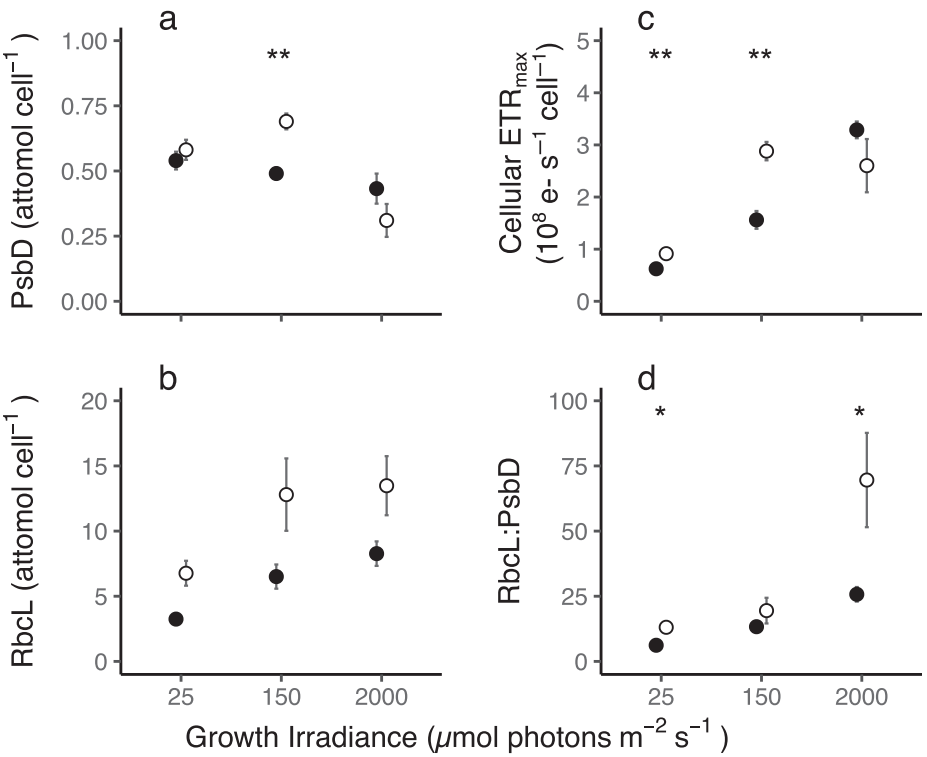

Fig. 4. Cellular photosynthetic protein and energy quotas. Mean quotas of PsbD (**a**) and RbcL (**b**) and cell-normalized maximum electron transport rates, ETR_{max} (**c**), and RbcL : PsbD ratios (**d**) for naked (closed) and calcified (open) cells, respectively, grown at 25, 150, and 2000 μmol photons m^{-2} s^{-1}. Data represent the mean and standard error ($n = 2$–6). Asterisks indicate pairwise statistical differences (*$p < 0.05$; **$p < 0.01$; ***$p < 0.001$) between naked and calcified cell cultures. Statistical comparisons across irradiances are available in Supporting Information Dataset S1.

(0.31 ± 0.06 amol cell^{-1}) compared to LL and ML (0.58 ± 0.04 and 0.69 ± 0.03 amol cell^{-1}, respectively; Fig. 4a; Supporting Information Dataset S1). Notably, calcified cells had higher PsbD quotas at ML than naked cells (0.69 ± 0.03 vs. 0.49 ± 0.02 amol cell^{-1}, respectively; *t*-test *p*-value < 0.01). Cellular RbcL quotas increased with irradiance in naked cells from 3.3 ± 0.04 at LL to 8.3 ± 0.9 amol cell^{-1} at HL (ANOVA *p*-value < 0.05; Tukey HSD *p*-value < 0.05). Calcified cells had cellular RbcL quotas ranging from 6.8 ± 1.0 to 13.5 ± 2.3 amol cell^{-1} across irradiance (Fig. 4b). RbcL quotas were statistically indistinguishable between calcified and naked cells across irradiance (Fig. 4b; Supporting Information Dataset S1).

Cell-normalized maximum electron transport rates (cellular ETR_{max}) were calculated using the cellular PSII quotas. Cellular ETR_{max} increased with irradiance in naked cells from $6.2 \times 10^7 \pm 5.0 \times 10^6$ e^- s^{-1} cell^{-1} at LL to $3.3 \times 10^8 \pm 1.6 \times 10^7$ e^- s^{-1} cell^{-1} at HL (ANOVA *p*-value < 0.001; Tukey HSD *p*-value < 0.001; Fig. 4d). Cellular ETR_{max} also increased in calcified cells, from $9.1 \times 10^7 \pm 3.4 \times 10^6$ e^- s^{-1} cell^{-1} at LL to $2.9 \times 10^8 \pm 1.8 \times 10^7$ e^- s^{-1} cell^{-1} at ML (ANOVA *p*-value < 0.05; Tukey HSD *p*-value < 0.05) and remained high at HL ($2.6 \times 10^8 \pm 5.1 \times 10^7$ e^- s^{-1} cell^{-1}; Fig. 4d). Cellular ETR_{max} was 1.5- and 1.9-fold higher in calcified cells than naked cells at LL and ML, respectively (*t*-test *p*-value < 0.01). Mean RbcL : PsbD increased with irradiance in naked cells (*p*-value < 0.05) but was > 2-fold higher in calcified cells than naked cells at LL (13.1 ± 1.5 vs. 6.2 ± 0.45, respectively) and HL (69.6 ± 18.1 vs. 28.5 ± 0.63, respectively; *t*-test *p*-value < 0.05).

Particulate carbon production

The 3 h, $^{14}C - HCO_3^-$ incubations in the light produced PIC production rates ranging from 0.27 ± 0.05 pg C cell^{-1} h^{-1} at LL to 0.76 ± 0.20 pg C cell^{-1} h^{-1} at HL (Fig. 5a; Supporting Information Dataset S1). The rate of POC fixation was similar in naked cells at LL and ML (0.13 ± 0.004 and 0.26 ± 0.09 pg C cell^{-1} h^{-1}, respectively) but increased ~2- to 4-fold at HL (0.54 ± 0.002 pg C cell^{-1} h^{-1}) relative to LL and ML (ANOVA *p*-value < 0.01; Tukey HSD *p*-value < 0.05). Particulate organic carbon fixation in calcified cells increased from 0.32 ± 0.06 pg C cell^{-1} h^{-1} at LL to 1.0 ± 0.03 pg C cell^{-1} h^{-1} at ML (ANOVA *p*-value < 0.05, Tukey HSD *p*-value < 0.05), remaining elevated (1.3 ± 0.26 pg C cell^{-1} h^{-1}) at HL. Calcified cells fixed ~2.5-fold more POC than naked cells at LL (*t*-test *p*-value < 0.01) and at HL (*t*-test *p*-value < 0.05); this increased to a ~4-fold higher POC fixation rate at ML (*t*-test *p*-value < 0.001; Fig. 5b; Supporting Information Dataset S1). Particulate inorganic carbon production was fractionally lower than POC

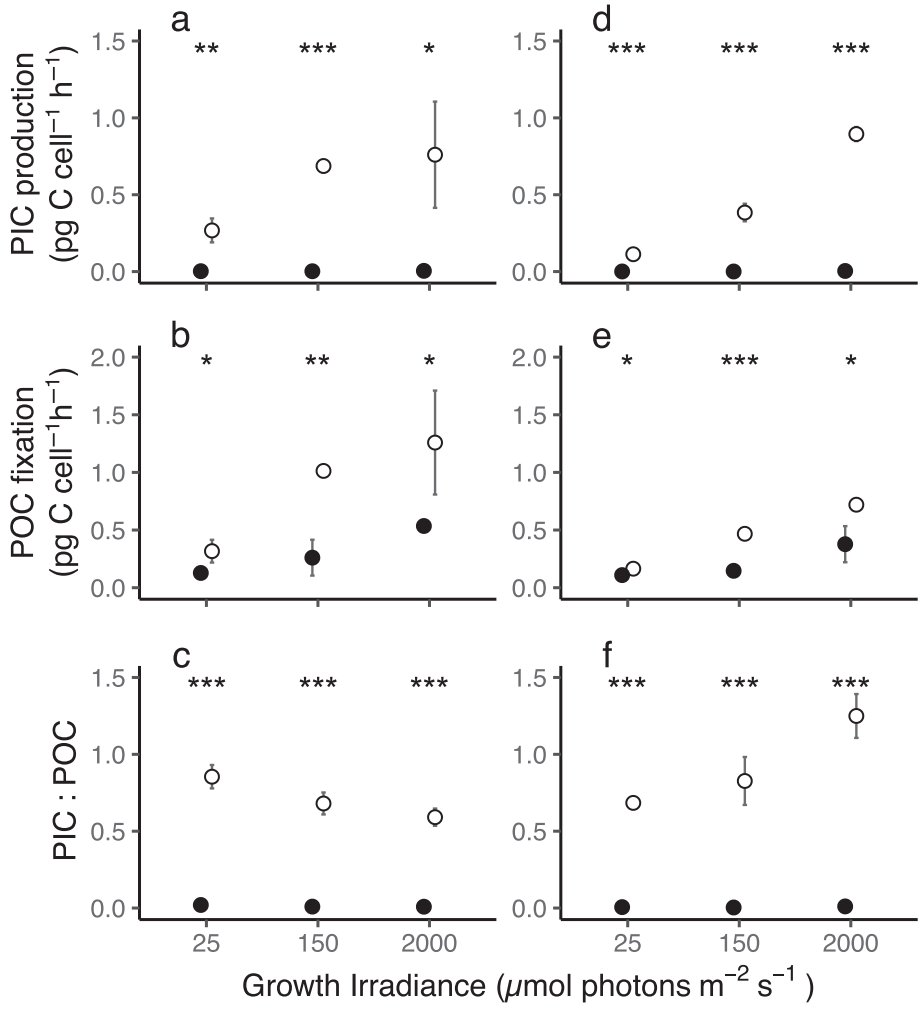

Fig. 5. Particulate inorganic carbon (PIC) and particulate organic carbon (POC) production rates. PIC (**a**, **d**) and POC (**b**, **e**) production rates for naked (closed) and calcified (open) cells grown at 25, 150, and 2000 μmol photons m^{-2} s^{-1} for 3 h (**a**–**c**) and 24 h (**d**–**f**) incubation experiments. Mean PIC : POC production ratio (**c**, **f**) for calcified cells is shown. Data are mean and standard error ($n = 3$). Asterisks indicate pairwise statistical differences (*$p < 0.05$; **$p < 0.01$; ***$p < 0.001$) between naked and calcified cell cultures. Statistical comparisons across irradiances are available in Supporting Information Dataset S1.

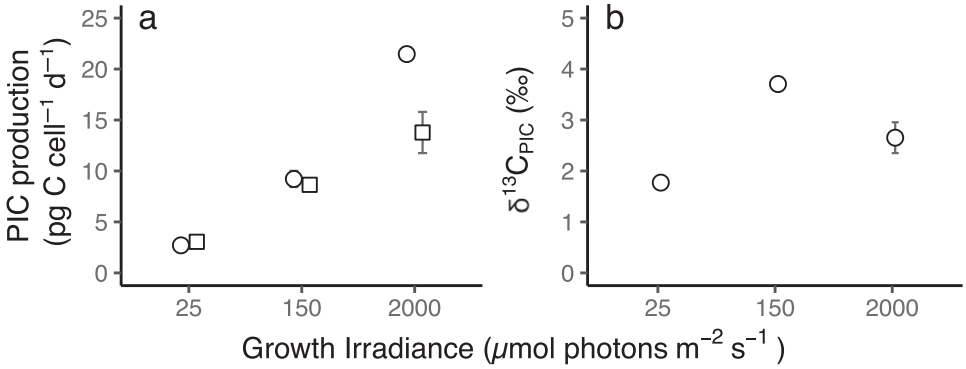

Fig. 6. Calcite production and characteristics. Particulate inorganic carbon (PIC) production rates (**a**) determined via alkalinity drawdown (squares) compared to rates determined via 24-h ^{14}C incubations (circles) and δ^{13}C values of PIC (**b**) for calcified cells grown at 25, 150, and 2000 μmol photons m^{-2} s^{-1}. Data are mean and standard error ($n = 3$). Statistical comparisons across irradiances (ANOVA and post hoc comparisons) are available in Supporting Information Dataset S1.

fixation across irradiances (~0.86× at LL, ~0.68× at ML, and ~0.59× at HL; Fig. 5c).

The 24 h, $^{14}C-HCO_3^-$ incubations over a LD cycle resulted in PIC and POC production rates with similar trends across irradiances compared to the 3-h rates (Fig. 5; Supporting Information Dataset S1). In calcified cells, the rate of PIC production was lowest at LL (0.11 ± 0.004 pg C cell^{-1} h^{-1}) and increased ~3.5-fold at ML (0.38 ± 0.03 pg C cell^{-1} h^{-1}; ANOVA p-value <0.001; Tukey HSD p-value <0.001) and another ~2.5-fold at HL (0.90 ± 0.03 pg C cell^{-1} h^{-1}; Tukey HSD p-value <0.001; Fig. 5d). The rate of POC fixation in naked cells was similar at LL and ML (0.11 ± 0.02 and 0.15 ± 0.02 pg C cell^{-1} h^{-1}, respectively) and increased ~2.5- to 3.5-fold to 0.38 ± 0.09 pg C cell^{-1} h^{-1} at HL (ANOVA p-value <0.05; Tukey HSD p-value <0.05). Particulate organic carbon fixation in calcified cells increased with irradiance (ANOVA p-value <0.001) and was ~1.5- to 3-fold higher at LL (0.17 ± 0.002 pg C cell^{-1} h^{-1}; t-test p-value <0.05), ML (0.47 ± 0.01 pg C cell^{-1} h^{-1}; t-test p-value <0.001), and HL (0.72 ± 0.03 pg C cell^{-1} h^{-1}; t-test p-value <0.05) than POC fixation in naked cells (Fig. 5e). PIC production was ~0.68 and ~0.83 of POC fixation at LL and ML, respectively, but increased to ~1.25 of POC fixation at HL (Fig. 5f).

Carbonate chemistry analysis of culture media during growth showed greater reductions in alkalinity and DIC concentrations in calcified cultures relative to naked cultures (Supporting Information Fig. S6; Dataset S1). Calcified cells drew down ~18–41% more DIC per cell than naked cells across irradiance levels (Supporting Information Fig. S6). PIC production rates calculated from alkalinity drawdown after 2 d of growth corroborated 24-h PIC production rates determined from $^{14}C-HCO_3^-$ incubation experiments; 3.1 ± 0.17 pg C cell^{-1} d^{-1} at LL, 8.6 ± 0.11 pg C cell^{-1} d^{-1} at ML, and 13.8 ± 2.0 pg C cell^{-1} d^{-1} at HL (Fig. 6a). PIC was also enriched in ^{13}C relative to the growth media (Fig. 6b). Background corrected $\delta^{13}C_{PIC}$ values varied across irradiances (ANOVA p-value <0.01); it was least enriched at LL ($1.8‰ \pm 0.12‰$) and more enriched at higher irradiances ($3.7‰ \pm 0.14‰$ at ML and $2.7‰ \pm 0.30‰$ at HL; Tukey HSD p-value <0.001 and p-value <0.05, respectively; Figure 6b), where measured calcification rates were also highest.

The fate of coccoliths

The coccolith production rate (*see* Materials and Methods) was lowest at LL (~0.90 coccoliths cell^{-1} h^{-1}), increasing 3.8- and 3.1-fold at ML and HL, respectively (Table 1). Coccolith shedding rates (*see* Materials and Methods) were lowest at LL and HL (0.21 ± 0.03 and 0.35 ± 0.06 coccoliths cell^{-1} h^{-1}, respectively) and increased ~3- to 6-fold to 1.2 ± 0.06 coccoliths cell^{-1} h^{-1} at ML (ANOVA p-value <0.001, Tukey HSD p-value <0.01; Fig. 7; Supporting Information Fig. S7; Table 1). Assuming constant coccolith shedding rates and PIC production rates over the light period, this translated into cells

Table 1. Coccolith and particulate inorganic carbon (PIC) dynamics during the light period. Coccolith PIC content (pg C coccolith^{-1}, mean ± standard error) and PIC quotas (*see* Fig. 1, mean ± standard error) were used to determine the coccolith (attached and free) cell quota (coccoliths cell^{-1}). The PIC loss (pg C cell^{-1}) and the fraction of PIC produced and lost (dimensionless) during the light period (14 h) was determined from the coccolith shedding rate (coccoliths cell^{-1} h^{-1}, mean ± standard error), 3-h PIC production rate (pg C cell^{-1} h^{-1}), and coccolith PIC content. Coccoliths per daughter cell (coccoliths cell^{-1}) was calculated from the number of coccoliths that remained attached at the end of the light period and the doubling time of calcified cells, with coccosphere PIC quota (pg C cell^{-1} h^{-1}) being the corresponding PIC quota (*see* Materials and Methods).

Growth irradiance	Coccolith PIC content	Coccolith production rate	Coccolith (attached + free) cell quota	Coccolith shedding rate	PIC loss	Fraction of PIC lost	Coccoliths per daughter cell	Coccosphere PIC quota
25 (LL)	0.30 ± 0.02	0.90 (*0.80–1.0*)	11.5 (*10.0–12.9*)	0.21 ± 0.03	0.86 (*0.71–1.02*)	0.23 (–)	12.3 (*9.8–16.3*)	3.7 (*2.8–5.1*)
150 (ML)	0.20 ± 0.02	3.5 (*3.3–3.6*)	42.1 (*40.5–43.4*)	1.2 ± 0.06	3.3 (*2.9–3.7*)	0.34 (*0.31–0.37*)	11.0 (10.9–11.3)	2.2 (*2.1–2.3*)
2000 (HL)	0.27 ± 0.02	2.8 (*2.2–3.4*)	32.2 (*31.8–32.7*)	0.35 ± 0.06	1.3 (*1.1–1.7*)	0.13 (*0.12–0.13*)	14.8 (*10.7–19.6*)	4.0 (*2.7–5.6*)

Note: Italicized values represent the range in data measurements.

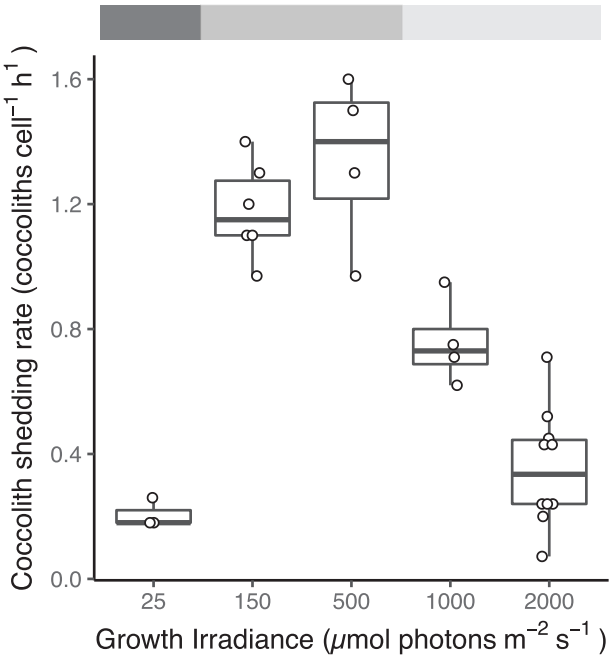

Fig. 7. Coccolith shedding rates. Coccolith shedding rates for calcified cells grown at 25–2000 μmol photons m^{-2} s^{-1}, with low light (LL, dark gray), medium light (ML, medium gray), and high light (HL, light gray) indicated by shaded gradient bars. Boxplots represent distributions of 3–10 replicates across each irradiance level. Upper and lower bounds of each box plot represent the 25% and 75% percentiles around the median, with whiskers representing data that are ≤ 1.5 times the interquartile range. Statistical comparisons across irradiances (ANOVA and post hoc comparisons) are available in Supporting Information Dataset S1.

discarding similar amounts of PIC at LL and HL (~ 0.86 and ~ 1.33 pg C cell^{-1}, respectively), equating to ~ 23% and ~ 13% of PIC produced, respectively. Discarded PIC at ML increased to ~ 3.28 pg C cell^{-1}, accounting for ~ 34% of the PIC produced during the light period (Table 1). Newly produced daughter cells were estimated to inherit 11.0–14.8 coccoliths cell^{-1}, after accounting for this loss (Table 1).

Discussion

Light intensity and calcification drive growth and photophysiological responses

Growth, Chl *a* concentration and photosynthetic parameters followed expected trends across irradiance in both naked and calcified cells. Growth was maximal at ML (150–500 μmol photons m^{-2} s^{-1}) and lower at LL and HL. Decreased Chl *a*, F_v/F_m, σ_{PSII}, and α, and increased E_k, ETR_{max} per PSII, and NPQ were observed for each phenotype from LL to HL. Nonphotochemical quenching showed no relationship with PIC production rate; PIC production rates were similarly high at ML and HL, while NPQ scaled strongly with light. Based on ETR per PSII, the LR of photosynthesis appeared to saturate at 500 μmol photons m^{-2} s^{-1} in both naked and calcified cells. However, higher PSII quotas in calcified cells compared to naked cells at 150 μmol photons m^{-2} s^{-1} suggest cellular ETR in calcified cells saturated at this lower irradiance.

Despite similar trends *across* irradiance, calcified cells exhibited 11–13% higher growth rates than naked cells *within* irradiance at 150, 1000, and 2000 μmol photons m^{-2} s^{-1}. This was supported by higher rates of POC fixation, with discernable differences across irradiance hinting at different underlying mechanisms. Higher PSII quotas in calcified cells at ML appeared to drive higher rates of cellular ETR_{max}; at the same time, ~ 3-fold higher RbcL : PsbD ratio in calcified cells likely supported higher POC fixation at HL (given similar cellular ETR_{max} between phenotypes at this irradiance). We argue that the effective scattering and reduction of light intensity by coccoliths at HL allowed cells to maintain higher σ_{PSII} and more efficiently convert harvested light energy into chemical energy (higher α) compared to naked cells. This feature is further facilitated by very low coccolith shedding rates at HL and tight maintenance of the coccosphere (*see* below).

Calcification and coccolith retention are dependent on light intensity

The degree of calcification (i.e., cellular PIC quota) increased from LL to ML (25–150 μmol photons m^{-2} s^{-1}) but saturated at 150 μmol photons m^{-2} s^{-1}. This corroborates previous studies reporting increased calcification with irradiance prior to saturation at 70–80 μmol photons m^{-2} s^{-1};(van Bleijswijk et al. 1994; Zondervan et al. 2002). Despite low rates of calcification (i.e., PIC and coccolith production rates) at 25 μmol photons m^{-2} s^{-1}, cells maintained a complete coccosphere (~ 12 coccoliths; Table 1) aided by minimal loss of coccoliths through shedding. These results are similar to previous findings that calcification in *E. huxleyi* is light limited at < 30 μmol photons m^{-2} s^{-1} (Raven and Crawfurd 2012). Conversely, cells at ML (150 μmol photons m^{-2} s^{-1}) had high rates of calcification but cells discarded ~ 34% of the PIC produced via coccolith shedding (Table 1). This hints at a cellular benefit of coccolith production that outweighs the energetic cost of increased calcification and is not dependent on coupled incorporation into the coccosphere.

Similarly high 3-h PIC production rates and PIC quotas at HL and ML suggested both the rate and degree of calcification was saturated, similar to previous studies (Balch et al. 1992; Trimborn et al. 2007; Barcelos e Ramos et al. 2012), but not photoinhibited (as suggested by Feng et al. 2008). At the same time, the coccolith shedding was ~ 3-fold lower at HL demonstrating that high coccolith production does not inherently translate into increased coccolith shedding. Taken together with observations that HL cells had the highest coccolith quota (~ 15 coccoliths), it points to a light-dependent cellular mechanism whereby cells at HL retain coccoliths within the coccosphere, perhaps for optical protection. The cellular mechanism(s) of this differential shedding remain unknown and underly light-related controls on coccosphere maintenance.

Proposed role of calcification in *E. huxleyi*

Our data demonstrate a photoprotective role for calcification with coccoliths acting to scatter light and reduce light intensity entering the cell, consistent with previous studies showing that coccoliths scatter light (Mizukawa et al. 2015) and reduce visible light by 7.5–22% (Gao et al. 2009; Xu et al. 2016). Though naked cells in our study and in previous studies (Paasche 2002; Harris et al. 2005) have shown

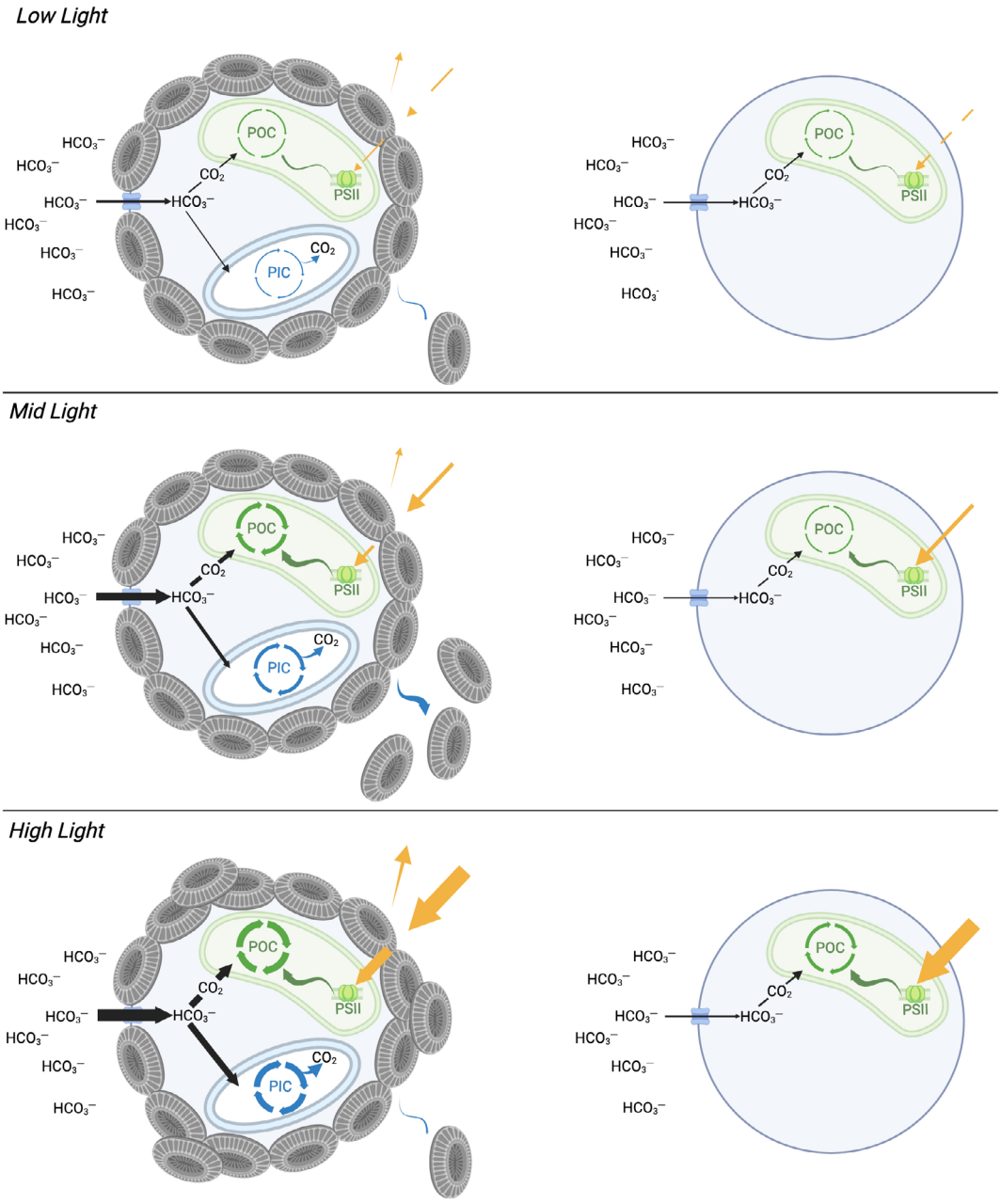

Fig. 8. Differential carbon cell investments for *Emiliania huxleyi* phenotypes across irradiance. Relative changes in bicarbonate uptake, photosynthesis, and calcification in calcified (left) and naked (right) cells across low, mid, and high light (reflected as yellow arrows entering cell). Bicarbonate is taken up and is transported to the plastid or coccolith vesicle to be utilized by photosynthesis (after conversion to CO_2) or calcification, respectively (black arrows). Photosynthesis occurring in the plastid is depicted as energy transport from photosystem II (PSII, green curved arrow) and particulate organic carbon fixation (POC, green arrow circles). Calcification is depicted as particulate inorganic carbon production (PIC, blue arrow circles) occurring in the coccolith vesicle (with 1 mol CO_2 produced per mol PIC) and coccolith shedding (blue curved arrow). Coccoliths also scatter light (yellow arrow leaving coccolith), reducing the intensity of light that reaches photosystem (yellow arrow reaching PSII in calcified cells). Arrow thickness indicate relative values. Created with BioRender.com.

resistance to photoinhibition at high irradiance, calcification appears to further enhance protection from photoinhibition by scattering light.

Calcified cells drew down more DIC than naked cells across irradiance (Supporting Information Fig. S6), which supported higher POC fixation. They also devoted more resources to POC fixation than PIC production. Our data support a role for calcification in increasing intracellular HCO_3^- supply for photosynthesis. Previous studies have suggested that CO_2 produced during calcification can be used for photosynthesis (Sikes et al. 1980; Anning et al. 1996; Hoppe et al. 2011), but others have suggested the two processes compete for HCO_3^- (Mackinder et al. 2011; Bach et al. 2013; Bolton and Stoll 2013). Given that the RuBisCO discrimination value against ^{13}C is 11.1‰ (Boller et al. 2011), the intracellular HCO_3^- pool available for calcification should be enriched in ^{13}C (McClelland et al. 2017). We found calcite $\delta^{13}C$ enrichment was higher in cells growing at irradiances where photosynthesis was saturated, with the highest values at ML coinciding with high growth, calcification, and POC fixation rates. This argues that calcification and photosynthesis were drawing from the same internal HCO_3^- pool. At the same time, cells maintained sufficiently high pCO_2 levels and avoided CO_2 limitation of photosynthesis. We posit that under non-limiting HCO_3^- concentrations, calcification acts to effectively concentrate cellular carbon for photosynthesis by facilitating increased supply and intracellular HCO_3^- pools.

Proposed model of light-dependent calcification and carbon fixation in *E. huxleyi*

We propose a cellular model of light-dependent calcification and carbon fixation that integrates across our multifaceted datasets (Fig. 8). Calcification increases bicarbonate uptake and supply for the DR of photosynthesis and POC fixation. Bicarbonate uptake and supply would further increase with light, given PIC production scales accordingly. This advantage of calcification to POC fixation is even afforded to cells under conditions limiting for growth and photosynthesis (LL; 25 μmol photons m^{-2} s^{-1}); indeed, cells maintain a complete coccosphere (~ 12 coccoliths) despite scattering effects. The photoprotective role of coccolith scattering at HL leads cells to efficiently retain coccoliths in the coccosphere by a yet unknown mechanism. Optimal growth at mid-light levels fuels high rates of calcification and concomitant increases in bicarbonate supply to support high photosynthetic and the highest growth rates. These cellular benefits outweigh the cost of discarding a large fraction (~ 34%) of PIC via shedding. Thus, calcification serves tandem carbon concentrating and photoprotective roles that enhance photosynthesis and growth, as cells maintain basal coccosphere quotas of 11–15 coccoliths and the production and fate (attached or shed) of coccoliths being determined by irradiance.

Calcified cells inherently have higher carbon, energetic, and physiological requirements compared to naked cells. Although the cost of HCO_3^- transport (extracellular and intracellular) for calcification is small, at an estimated ~ 5% of photosynthetic energy (Monteiro et al. 2016), and is outweighed by the subsequent increase in organic carbon fixation, the costs of calcification extend beyond just investments in HCO_3^- transport. We posit that calcified cells increase cellular photosynthetic output at and above a mid-light optimum in order to generate additional energy to support calcification, such as synthesis of ion transporters (Ca^{2+} and H^+ in addition to HCO_3^-) and coccolith-associated polysaccharides (CAPs), proteins and lipids (Johns et al. 2019; Skeffington et al. 2023; Mackinder et al. 2010; Kegel et al. 2013). Cellular investments in ion transport are estimated at 13–30% of the total photosynthetic energy budget in *E. huxleyi* (Raven and Crawfurd 2012; Monteiro et al. 2016). CAP synthesis is estimated to use ~ 7–23% of fixed carbon (Kayano and Shiraiwa 2009; Tsuji et al. 2015; Monteiro et al. 2016; Taylor et al. 2017; Wilkes et al. 2018).

Our findings that calcified cells discard up to ~ 1/3 of PIC produced at mid-light points to a dynamic balance between cellular resources and costs. There are likely light-dependent investments in biochemical processes and cellular machinery (e.g., pentose phosphate pathway, antioxidant pathways) related to calcification that increase the energetic demand(s) of calcified cells relative to naked cells. The observed differences in both POC and PIC production between the 3- and 24-h incubations are noteworthy and reflect metabolic and/or chemical losses into from respective pools, conceptually akin to differences in gross and net production. While mitochondrial respiration and dissolution can contribute to these differences, there are additional factors to consider. First, POC and PIC production are lower in the dark (Müller et al. 2008), so the 24-h production rates (which integrate the 10-h dark period) are expected to be lower than the 3-h rates. Secondly, calcified *E. huxleyi* cells have been shown to exude ~ 41% more photosynthetically fixed carbon to DOC via exudation than naked cells during exponential growth at ML (Diaz et al. 2023). Third, pH driven impacts on PIC dissolution over this time period are unlikely. Direct measurements of mitochondrial respiration, exudation, and dissolution are warranted in subsequent work. Future analyses should identify and quantify the array of energetic costs and differential cellular investments across phenotypes and irradiances. This would enhance our understanding of how calcification impacts the ability of coccolithophores to adapt to changing light regimes with relevance to the fixation and fate of carbon in a mixing water column.

Data availability statement

Data that support the findings of this study are available in Supporting Information Dataset S1.

References

Anning, T., N. Nimer, M. J. Merrett, and C. Brownlee. 1996. Costs and benefits of calcification in coccolithophorids. J. Mar. Syst. **9**: 45–56. doi:10.1016/0924-7963(96)00015-2

Armstrong, R. A., C. Lee, J. I. Hedges, S. Honjo, and S. G. Wakeham. 2001. A new, mechanistic model for organic carbon fluxes in the ocean based on the quantitative association of POC with ballast minerals. Deep-Sea Res. II Topic. Stud. Oceanogr. **49**: 219–236. doi:10.1016/S0967-0645(01)00101-1

Bach, L. T., and others. 2013. Dissecting the impact of CO_2 and pH on the mechanisms of photosynthesis and calcification in the coccolithophore *Emiliania huxleyi*. New Phytol. **199**: 121–134. doi:10.1111/nph.12225

Balch, W., D. Drapeau, B. Bowler, and E. Booth. 2007. Prediction of pelagic calcification rates using satellite measurements. Deep-Sea Res. II Top. Stud. Oceanogr. **54**: 478–495. doi:10.1016/j.dsr2.2006.12.006

Balch, W. M., P. M. Holligan, and K. A. Kilpatrick. 1992. Calcification, photosynthesis and growth of the bloom-forming coccolithophore, *Emiliania huxleyi*. Cont. Shelf Res. **12**: 1353–1374. doi:10.1016/0278-4343(92)90059-S

Balch, W. M., K. A. Kilpatrick, and C. C. Trees. 1996. The 1991 coccolithophore bloom in the central North Atlantic.1. Optical properties and factors affecting their distribution. Limnol. Oceanogr. **41**: 1669–1683. doi:10.4319/lo.1996.41.8.1669

Balch, W. M., D. T. Drapeau, and J. J. Fritz. 2000. Monsoonal forcing of calcification in the Arabian Sea. Deep-Sea Res. II Top. Stud. Oceanogr. **47**: 1301–1337. doi:10.1016/S0967-0645(99)00145-9

Barcelos e Ramos, J., K. Schulz, S. Febiri, and U. Riebesell. 2012. Photoacclimation to abrupt changes in light intensity by *Phaeodactylum tricornutum* and *Emiliania huxleyi*: The role of calcification. Mar. Ecol. Prog. Ser. **452**: 11–26. doi:10.3354/meps09606

Berelson, W. M., W. M. Balch, R. Najjar, R. A. Feely, C. Sabine, and K. Lee. 2007. Relating estimates of $CaCO_3$ production, export, and dissolution in the water column to measurements of $CaCO_3$ rain into sediment traps and dissolution on the sea floor: A revised global carbonate budget. Global Biogeochem. Cycl. **21**: 15.

Bilger, W., and O. Björkman. 1990. Role of the xanthophyll cycle in photoprotection elucidated by measurements of light-induced absorbance changes, fluorescence and photosynthesis in leaves of Hedera canariensis. Photosynth. Res. **25**: 173–185. doi:10.1007/BF00033159

Boller, A. J., P. J. Thomas, C. M. Cavanaugh, and K. M. Scott. 2011. Low stable carbon isotope fractionation by coccolithophore RubisCO. Geochim. Cosmochim. Acta **75**: 7200–7207. doi:10.1016/j.gca.2011.08.031

Bolton, C. T., and H. M. Stoll. 2013. Late Miocene threshold response of marine algae to carbon dioxide limitation. Nature **500**: 558–562. doi:10.1038/nature12448

Broecker, W., and E. Clark. 2009. Ratio of coccolith $CaCO_3$ to foraminifera $CaCO_3$ in late Holocene deep sea sediments. Paleoceanography **24**: 11.

Brown, C. M., J. D. MacKinnon, A. M. Cockshutt, T. A. Villareal, and D. A. Campbell. 2008. Flux capacities and acclimation costs in Trichodesmium from the Gulf of Mexico. Mar. Biol. **154**: 413–422. doi:10.1007/s00227-008-0933-z

Buitenhuis, E. T., H. J. W. De Baar, and M. J. W. Veldhuis. 1999. Photosynthesis and calcification by *Emiliania huxleyi* (Prymnesiophyceae) as a function of inorganic carbon species. J. Phycol. **35**: 949–959. doi:10.1046/j.1529-8817.1999.3550949.x

de Jong, E. W., L. Bosch, and P. Westroek. 1976. Isolation and characterization of a cat 2+-binding polysaccharide associated with coccoliths of *Emiliania huxleyi* (Lohmann) Kamptner. Eur. J. Biochem. **70**: 611–621. doi:10.1111/j.1432-1033.1976.tb11052.x

Diaz, B. P., F. Gallo, R. H. Moore, and K. D. Bidle. 2023. Virus infection of phytoplankton increases average molar mass and reduces hygroscopicity of aerosolized organic matter. Sci. Rep. **13**: 7361. doi:10.1038/s41598-023-33818-4

Feng, Y., and others. 2008. Interactive effects of increased pCO_2, temperature and irradiance on the marine coccolithophore *Emiliania huxleyi* (Prymnesiophyceae). Eur. J. Phycol. **43**: 87–98. doi:10.1080/09670260701664674

Gal, A., R. Wirth, J. Kopka, P. Fratzl, D. Faivre, and A. Scheffel. 2016. Macromolecular recognition directs calcium ions to coccolith mineralization sites. Science. **353**: 590–593.

Gao, K., Z. Ruan, V. E. Villafañe, J.-P. Gattuso, and E. W. Helbling. 2009. Ocean acidification exacerbates the effect of UV radiation on the calcifying phytoplankter *Emiliania huxleyi*. Limnol. Oceanogr. **54**: 1855–1862. doi:10.4319/lo.2009.54.6.1855

Gorbunov, M. Y., and P. Falkowski. 2005. Fluorescence induction and relaxation (FIRe) technique and instrumentation for monitoring photosynthetic processes and primary production in aquatic ecosystems, p. 1029–1031. *In* A. van der Est and D. Bruce [eds.], Photosynthesis: Fundamental aspects to global perspectives. Proceedings of the 13th International Congress on Photosynthesis. Allen Press.

Guan, W., and K. Gao. 2010. Enhanced calcification ameliorates the negative effects of UV radiation on photosynthesis in the calcifying phytoplankter *Emiliania huxleyi*. Chin. Sci. Bull. **55**: 588–593. doi:10.1007/s11434-010-0042-5

Harris, G. N., D. J. Scanlan, and R. J. Geider. 2005. Acclimation of *Emiliania huxleyi* (Prymnesiophyceae) to photon flux density. J. Phycol. **41**: 851–862. doi:10.1111/j.1529-8817.2005.00109.x

Herfort, L., E. Loste, F. Meldrum, and B. Thake. 2004. Structural and physiological effects of calcium and magnesium in *Emiliania huxleyi* (Lohmann) Hay and Mohler. J. Struct. Biol. **148**: 307–314. doi:10.1016/j.jsb.2004.07.005

Hoppe, C. J. M., G. Langer, and B. Rost. 2011. *Emiliania huxleyi* shows identical responses to elevated pCO2 in TA and DIC

manipulations. J. Exp. Mar. Biol. Ecol. **406**: 54–62. doi:10.1016/j.jembe.2011.06.008

Iglesias-Rodríguez, M. D., and others. 2002. Representing key phytoplankton functional groups in ocean carbon cycle models: Coccolithophorids. Global Biogeochem. Cycl. **16**: 20.

Jassby, A. D., and T. Platt. 1976. Mathematical formulation of the relationship between photosynthesis and light for phytoplankton. Limnol. Oceanogr. **21**: 540–547. doi:10.4319/lo.1976.21.4.0540

Jeffrey, S. W., and G. F. Humphrey. 1975. New spectrophotometric equations for determining chlorophylls *a*, *b*, c_1 and c_2 in higher plants, algae and natural phytoplankton. Biochem. Physiol. Pflanz. **167**: 191–194. doi:10.1016/S0015-3796(17)30778-3

Johns, C. T., and others. 2019. The mutual interplay between calcification and coccolithovirus infection. Environ. Microbiol. **21**: 1896–1915. doi:10.1111/1462-2920.14362

Johns, C. T., and others. 2023. Adsorptive exchange of coccolith biominerals facilitates viral infection. Sci. Adv. **9**: eadc8728. doi:10.1126/sciadv.adc8728

Kayano, K., and Y. Shiraiwa. 2009. Physiological regulation of coccolith polysaccharide production by phosphate availability in the coccolithophorid *Emiliania huxleyi*. Plant Cell Physiol. **50**: 1522–1531. doi:10.1093/pcp/pcp097

Kegel, J. U., U. John, K. Valentin, and S. Frickenhaus. 2013. Genome variations associated with viral susceptibility and calcification in *Emiliania huxleyi*. PLoS One **8**: 9.

Kitajima, M., and W. L. Butler. 1975. Quenching of chlorophyll fluorescence and primary photochemistry in chloroplasts by dibromothymoquinone. Biochim. Biophys. Acta (BBA) Bioenerg. **376**: 105–115. doi:10.1016/0005-2728(75)90209-1

Klaas, C., and D. E. Archer. 2002. Association of sinking organic matter with various types of mineral ballast in the deep sea: Implications for the rain ratio. Global Biogeochem. Cycl. **16**: 14.

Kottmeier, D. M., S. D. Rokitta, P. D. Tortell, and B. Rost. 2014. Strong shift from HCO_3^- to CO_2 uptake in *Emiliania huxleyi* with acidification: New approach unravels acclimation versus short-term pH effects. Photosynth. Res. **121**: 265–275. doi:10.1007/s11120-014-9984-9

Krumhardt, K. M., N. S. Lovenduski, M. D. Iglesias-Rodriguez, and J. A. Kleypas. 2017. Coccolithophore growth and calcification in a changing ocean. Prog. Oceanogr. **159**: 276–295. doi:10.1016/j.pocean.2017.10.007

Lyon, D. G. 2014. The effects of coccoliths on photosynthesis in *Emiliana huxleyi*. Thesis. The State Univ. of New Jersey.

Mackinder, L., G. Wheeler, D. Schroeder, U. Riebesell, and C. Brownlee. 2010. Molecular mechanisms underlying calcification in coccolithophores. Geomicrobiol. J. **27**: 585–595. doi:10.1080/01490451003703014

Mackinder, L., G. Wheeler, D. Schroeder, P. von Dassow, U. Riebesell, and C. Brownlee. 2011. Expression of biomineralization-related ion transport genes in *Emiliania huxleyi*. Environ. Microbiol. **13**: 3250–3265. doi:10.1111/j.1462-2920.2011.02561.x

McClelland, H. L. O., J. Bruggeman, M. Hermoso, and R. E. M. Rickaby. 2017. The origin of carbon isotope vital effects in coccolith calcite. Nat. Commun. **8**: 14511.

Mizukawa, Y., Y. Miyashita, M. Satoh, Y. Shiraiwa, and M. Iwasaka. 2015. Light intensity modulation by coccoliths of *Emiliania huxleyi* as a micro-photo-regulator. Sci. Rep. **5**: 13577.

Monteiro, F. M., and others. 2016. Why marine phytoplankton calcify. Sci. Adv. **2**: e1501822. doi:10.1126/sciadv.1501822

Müller, M. N., A. N. Antia, and J. LaRoche. 2008. Influence of cell cycle phase on calcification in the coccolithophore *Emiliania huxleyi*. Limnol. Oceanogr. **53**: 506–512. doi:10.4319/lo.2008.53.2.0506

Nam, O., Y. Shiraiwa, and E. Jin. 2018. Calcium-related genes associated with intracellular calcification of *Emiliania huxleyi* (Haptophyta) CCMP 371. Algae **33**: 181–189. doi:10.4490/algae.2018.33.4.21

Nanninga, H. J., and T. Tyrrell. 1996. Importance of light for the formation of algal blooms by *Emiliania huxleyi*. Mar. Ecol. Prog. Ser. **136**: 195–203. doi:10.3354/meps136195

Nimer, N. A., M. D. Iglesias-Rodriguez, and M. J. Merrett. 1997. Bicarbonate utilization by marine phytoplankton species. J. Phycol. **33**: 625–631. doi:10.1111/j.0022-3646.1997.00625.x

Paasche, E. 1964. A tracer study of the inorganic carbon uptake during coccolith formation and photosynthesis in the coccolithophorid *Coccolithus huxleyi*. Physiol. Plant. Suppl. **3**: 1–82.

Paasche, E. 1999. Reduced coccolith calcite production under light-limited growth: A comparative study of three clones of *Emiliania huxleyi* (Prymnesiophyceae). Phycologia **38**: 508–516.

Paasche, E. 2002. A review of the coccolithophorid *Emiliania huxleyi* (Prymnesiophyceae), with particular reference to growth, coccolith formation, and calcification–photosynthesis interactions. Phycologia **40**: 503–529.

Paasche, E., and S. Brubak. 1994. Enhanced calcification in the coccolithophorid *Emiliania huxleyi* (Haptophyceae) under phosphorus limitation. Phycologia **33**: 324–330.

Parsons, T. R., Y. Maita, and C. M. Lalli. 1984. A manual of chemical and biological methods for seawater analysis. Pergamon Press.

Raven, J., and K. Crawfurd. 2012. Environmental controls on coccolithophore calcification. Mar. Ecol. Prog. Ser. **470**: 137–166. doi:10.3354/meps09993

Read, B. A., and others. 2013. Pan genome of the phytoplankton *Emiliania* underpins its global distribution. Nature **499**: 209–213. doi:10.1038/nature12221

Ridgwell, A., and others. 2009. From laboratory manipulations to earth system models: Scaling calcification impacts of

ocean acidification. Biogeosciences **6**: 2611–2623. doi:10.5194/bg-6-2611-2009

Rost, B., and U. Riebesell. 2004. Coccolithophores and the biological pump: Responses to environmental changes, p. 99–125. *In* H. R. Thierstein and J. R. Young [eds.], Coccolithophores: From molecular processes to global impact. Springer.

Sikes, C. S., R. D. Roer, and K. M. Wilbur. 1980. Photosynthesis and coccolith formation: Inorganic carbon sources and net inorganic reaction of deposition1. Limnol. Oceanogr. **25**: 248–261. doi:10.4319/lo.1980.25.2.0248

Silsbe, G. M., and J. C. Kromkamp. 2012. Modeling the irradiance dependency of the quantum efficiency of photosynthesis. Limnol. Oceanogr. Methods **10**: 645–652. doi:10.4319/lom.2012.10.645

Skeffington, A., A. Fischer, S. Sviben, M. Brzezinka, M. Górka, L. Bertinetti, C. Woehle, B. Huettel, A. Graf, and A. Scheffel. 2023. A joint proteomic and genomic investigation provides insights into the mechanism of calcification in coccolithophores. Nat Commun. **14**: 3749.

Taylor, A. R., C. Brownlee, and G. Wheeler. 2017. Coccolithophore cell biology: Chalking up Progress. Ann. Rev. Mar. Sci. **9**: 283–310. doi:10.1146/annurev-marine-122414-034032

Thamatrakoln, K., and others. 2013. Death-specific protein in a marine diatom regulates photosynthetic responses to iron and light availability. Proc. Natl. Acad. Sci. USA **110**: 20123–20128. doi:10.1073/pnas.1304727110

Trimborn, S., G. Langer, and B. Rost. 2007. Effect of varying calcium concentrations and light intensities on calcification and photosynthesis in *Emiliania huxleyi*. Limnol. Oceanogr. **52**: 2285–2293. doi:10.4319/lo.2007.52.5.2285

Tsuji, Y., M. Yamazaki, I. Suzuki, and Y. Shiraiwa. 2015. Quantitative analysis of carbon flow into photosynthetic products functioning as carbon storage in the marine coccolithophore, *Emiliania huxleyi*. Mar. Biotechnol. **17**: 428–440. doi:10.1007/s10126-015-9632-1

Tyrrell, T., and A. Merico. 2004. Emiliania huxleyi: Bloom observations and the conditions that induce them. Springer, p. 75–97.

van Bleijswijk, J. D. L., R. S. Kempers, M. J. Veldhuis, and P. Westbroek. 1994. Cell and growth characteristics of types A and B of *Emiliania huxleyi* (Prymnesiophyceae) as determined by flow cytometry and chemical analysis. J. Phycol. **30**: 230–241. doi:10.1111/j.0022-3646.1994.00230.x

von Dassow, P., G. van den Engh, D. Iglesias-Rodriguez, and J. R. Gittins. 2012. Calcification state of coccolithophores can be assessed by light scatter depolarization measurements with flow cytometry. J. Plankton Res. **34**: 1011–1027. doi:10.1093/plankt/fbs061

Westbroek, P., and others. 1993. A model system approach to biological climate forcing. The example of *Emiliania huxleyi*. Global Planet. Change **8**: 27–46. doi:10.1016/0921-8181(93)90061-R

Wilkes, E. B., R. B. Y. Lee, H. L. O. McClelland, R. E. M. Rickaby, and A. Pearson. 2018. Carbon isotope ratios of coccolith–associated polysaccharides of *Emiliania huxleyi* as a function of growth rate and CO_2 concentration. Org. Geochem. **119**: 1–10. doi:10.1016/j.orggeochem.2018.02.006

Xu, J., L. T. Bach, K. G. Schulz, W. Zhao, K. Gao, and U. Riebesell. 2016. The role of coccoliths in protecting *Emiliania huxleyi* against stressful light and UV radiation. Biogeosciences **13**: 4637–4643. doi:10.5194/bg-13-4637-2016

Young, J. R., and K. Henriksen. 2003. Biomineralization within vesicles: The calcite of Coccoliths. Rev. Mineral. Geochem. **54**: 189–215. doi:10.2113/0540189

Ziveri, P., and others. 2023. Pelagic calcium carbonate production and shallow dissolution in the North Pacific Ocean. Nat. Commun. **14**: 805.

Zondervan, I., B. Rost, and U. Riebesell. 2002. Effect of CO_2 concentration on the PIC/POC ratio in the coccolithophore *Emiliania huxleyi* grown under light-limiting conditions and different daylengths. J. Exp. Mar. Biol. Ecol. **272**: 55–70. doi:10.1016/S0022-0981(02)00037-0

Acknowledgments

This work was made possible by support from the National Science Foundation (OIA-2021032 and OCE-1559179 to KDB and KT; OIA-020878 to AVS) and the Gordon and Betty Moore Foundation (Award # 3789 to KDB). The authors would also like to thank Maxim Gorbunov, Juan Bonachela, and William Balch for helpful discussions; Jason Latham, Liti Haramaty, Jozef Nissimov, and Frank Natale for technical assistance; and Ben Knowles and Karen Bondoc-Naumovitz for assistance with statistical analyses.

Conflict of Interest

None declared.

Submitted 13 February 2024
Revised 21 May 2024
Accepted 26 July 2024

Associate Editor: Katherina Petrou